Planet. Space Sci., Vol. 31, No. 2, pp. 197–206, 1983
Printed in Great Britain.

0032-0633/83/020197-10$03.00/0

DISSOCIATIVE EXCITATION OF SO_2 BY CONTROLLED ELECTRON IMPACT

K. BECKER, W. VAN WIJNGAARDEN and J. W. McCONKEY
Department of Physics, University of Windsor, Windsor, Ontario N9B 3P4, Canada

(*Received* 7 *July* 1982)

Abstract—The fragmentation of SO_2 following dissociative electron impact excitation has been studied under single collision conditions for incident electron energies up to 500 eV. The emission spectrum in the far v.u.v. spectral range (450–1100Å) shows many features arising from excited neutral oxygen and ionized oxygen and sulphur fragments. Absolute emission cross sections have been measured for the most intense lines and the maximum values were found to range from $1\text{–}12 \times 10^{-19}$ cm^2 with an uncertainty of approx. $\pm 35\%$. Dissociation mechanisms are discussed and in some cases the dissociation path could be uniquely identified. The striking differences between the v.u.v. emission spectrum produced by single step dissociation of SO_2 and the spectra emitted by the plasma torus around Jupiter are discussed.

1. INTRODUCTION

In January 1979, *Voyager* I at a distance of 1 AU from Jupiter, began observing the radiation in the range 500–1700Å emitted by the planetary system. Two bright emission lines in the vicinity of 685 and 833Å dominated the spectrum and it has been suggested (Broadford *et al.*, 1979; Sandel *et al.*, 1979) that ionized sulphur and oxygen species—in particular S III, S IV and O III—are the emitting sources. The peak intensity of the 685Å line, which is the overall most intense emission was found to occur at a distance of about five times the radius of the planet, which coincides with the orbital radius of Jupiter's satellite Io. At the same time *Voyager's* cameras photographed active volcanos on Io and, therefore, it appears very likely that the sulphur and oxygen ions result from the break-up of SO_2 molecules, which, when shot into orbit from the volcanoes, are dissociated and excited under photon and electron impact and form what is known as the "plasma torus" of the planet.

The present paper deals with the dissociative excitation of SO_2 by low energy electron impact under controlled single collision conditions in a laboratory crossed-beam experiment. Figure 1 shows a wavelength scan of the spectrum obtained. The most intense emission features observed in the spectral range from 450 to 1100Å were identified as arising from neutral or ionized oxygen and from ionized sulphur. Absolute emission cross sections are presented for the strongest emissions and in addition, detailed studies of the near threshold regions have been carried out to determine the onset potentials. A comparison of the measured onsets with the calculated minimum energies required for the emission of a particular line yields insight into the possible underlying dissociation mechanism(s).

To our knowledge the only other study of the dissociative excitation of SO_2 in the v.u.v. is the recent work of Srivastava and Ajello (1981) but this covers the wavelength range above 1100Å.

The fragmentation pattern of SO_2 has been the subject of previous investigations (see e.g. Smyth and Mueller, 1932 and Reese *et al.*, 1958) and numerous studies analysing the optical spectrum of SO_2 have been carried out (see e.g. refs. 5–16 quoted in the paper by Vuskovic and Trajmar, 1981). Recently, particularly with the *Voyager* fly-by missions to Jupiter and with the importance of sulphur dioxide as a major pollutant in our atmosphere, a new interest has arisen in SO_2. Electron impact techniques have been used to study the electronic energy levels and ionization continuum of the molecule (Foo *et al.*, 1971; Flicker *et al.*, 1978; Vuskovic and Trajmar, 1981). Smith and Stevenson (1981) measured cross sections for formation of parent and fragment ions following electron impact and details of relaxation processes in photo-excited SO_2 have been reported by Dujardin and Leach (1981). The absolute emission cross sections for relevant dissociation processes in SO_2 given in this paper contribute to a detailed modelling of the processes in the Jupiter environment.

2. EXPERIMENTAL

2.1. *Apparatus*

The experimental set-up has already been described in detail in previous publications from this laboratory (Donaldson *et al.*, 1972; McConkey and Donaldson, 1973) and only a brief outline will be given here.

An electron beam (energy $E = 20\text{–}500$ eV, energy spread $\Delta E_{FWHM} \approx 0.8$ eV, typical current 40 μA at 50 eV) is fired at right angles through a beam of SO_2

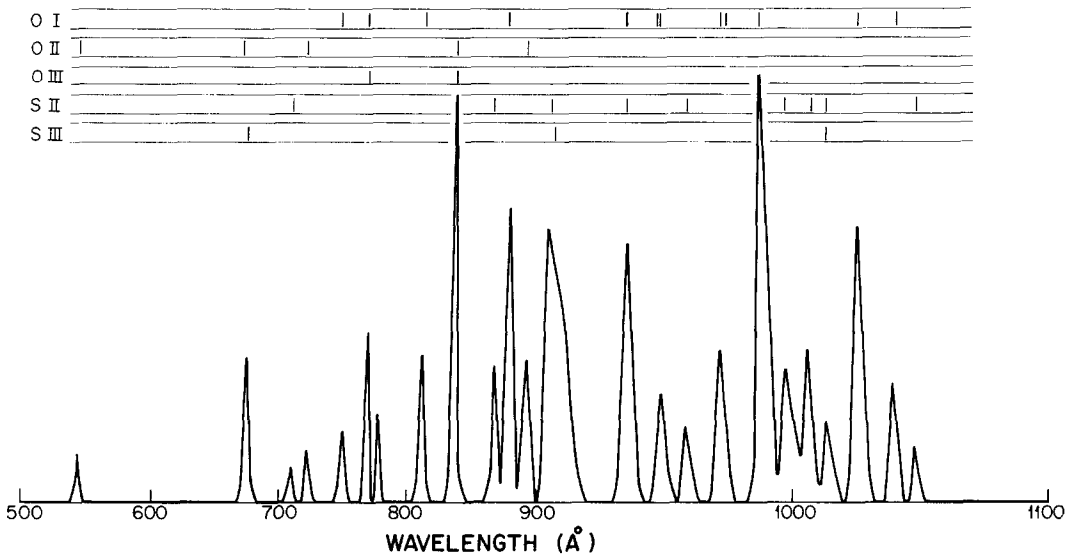

FIG. 1. V.U.V. SPECTRUM OF SO_2 EXCITED BY 100 eV ELECTRON IMPACT.
Identification of the different features is discussed in the text. Note the change in wavelength scale at 900 Å. The two halves of the spectrum were taken separately and thus the intensities above and below 900 Å should not be compared directly. Background noise has been subtracted for reasons of clarity. No correction for variation in detection efficiency with wavelength has been made.

molecules effusing from a multicapillary orifice (5500 holes, 0.002″ diameter). The number density of target molecules is continuously monitored by measuring the head pressure in the gas line with a MKS Baratron capacitance manometer. All measurements were performed in the molecular flow range where the beam number density is proportional to the head pressure. Except for measurements in the near threshold region, when a high number density of target molecules is essential to determine the onset potential of a line with reasonable precision, the chamber pressure was kept below 5×10^{-5} torr. With the beam off, the background pressure was 2×10^{-7} torr. The v.u.v. impact radiation observed perpendicular to both the electron and gas beams was dispersed in a Seya-Namioka spectrometer (grating 1200 grooves/mm, blazed at 700Å, reciprocal linear dispersion 17Å mm^{-1}) and detected by a channel-electron multiplier connected to a standard pulse-counting system.

As the lines to be studied lie close together in wavelength, it had to be ensured that only the required line was monitored. On the other hand, some emissions actually consisted of a blend of multiplets and we had to allow for the detection of the full features to enable a comparison of intensities. The appropriate slit widths were found, when a plot of signal intensity versus exit slit width displayed a plateau for a given entrance slit width (McConkey and Donaldson, 1972). Sometimes, however, the mutual separation of two broad emission features was comparatively small and we were not able to achieve a good plateau. As a consequence, an additional uncertainty was introduced to our data in these cases. The largest errors of this kind, estimated to be 10%, were found for the features at 974 and 682Å. In the first case we actually have two O I multiplets in the range 971.7–973.9Å and 976.5–978.6Å with a neighbouring O I multiplet of 6 lines centred at 989Å and in the second case two S III transitions at 680 and 683Å contribute to the 682Å peak with a O II line at 673Å close by.

2.2. *Procedure and sources of error*

For incident electron energies of 100 and 400 eV we scanned the wavelength over the region 450–1100Å using a resolution of 5Å (FWHM), see Fig. 1. The wavelength scale was calibrated against the well known positions of the resonance lines of the rare gases He I, Ne I and Ar I. Excitation functions were then recorded for the 19 most intense features from threshold (typically between 30 and 50 eV) up to 300 eV; for the 682Å S III and 539Å O II lines the energy range was extended to 500 eV, since in these cases the maximum of the excitation function occurred above 300 eV. In separate runs using a higher target gas pressure the near threshold region of each curve was covered in order to determine the appearance potentials. This could be

TABLE 1. CROSS-SECTION DATA OF RARE GAS LINES USED FOR THE NORMALIZATION OF EXCITATION FUNCTIONS

Species and wavelength	Apparent cross-section at 100 eV in 10^{-19} cm^2	Reference
He II 304Å	5.6*	Bloemen *et al.*, 1981
He I 522Å	10.7†	van Eck and de Jongh, 1970
	10.7	Donaldson *et al.*, 1972
He I 537Å	27.2	van Eck and de Jongh, 1970
	30.9	Donaldson *et al.*, 1972
	25.6	Westerveld *et al.*, 1979
He I 584Å	109.0	van Eck and de Jongh, 1970
	110.4	Donaldson *et al.*, 1972
	109.2	Westerveld *et al.*, 1979
Ne I 736Å	76.0	Tan *et al.*, 1974
Ar II 920Å	44.7‡	van Eck, 1971
	48.7	Tan *et al.*, 1974
Ar II 932Å	25.9‡	van Eck, 1971
	24.9	Tan *et al.*, 1974
Ar I 1048Å	245.5	McConkey and Donaldson, 1973
Ar I 1067Å	104.6	McConkey and Donaldson, 1973

* Emission cross-section at 200 eV incident energy.

† When more than one number is given for a particular line, the mean value was used for normalization.

‡ These numbers result from a private communication quoted in the paper of Tan *et al.* (1973).

done by the linear extrapolation of the increasing flank of the excitation function to within an accuracy of approx. ± 1.5 eV. The energy shift due to contact potentials was accounted for by calibrating the energy scale with respect to either the 21.2 eV onset of the He I $2^1P \rightarrow 1^1S$ resonance line or the 29.3 eV threshold for the emission of the Ar II line at 920Å. The excitation functions were then put on an absolute scale by comparison of the slopes of intensity vs head pressure plots with those of nearby lines of the rare gases whose cross sections were known. The reference lines and cross-sections used for the normalization are given in Table 1. Based on these data we were able to determine the relative quantum yield of our detection system at the corresponding wavelengths and to interpolate it over the wide spectral range of interest as shown in Fig. 2. The uncertainties in our cross-section data (see Tables 2a, 3, 4 and 5) consist first of all of the statistical error in the measurement of each excitation function (4–10%), which also takes into account fluctuations in target number density and electron current. Additional uncertainties arise from the normalization procedure, viz. the slopes of the intensity–pressure plots could be determined to within 3–5% for the rare gas lines and to within 8–12% for the S and O fragment emissions. If we also account for the finite accuracy of our interpolated quantum yield curve in Fig. 2, and if we recall that the rare gas cross-section data themselves are only given within a certain precision, then the overall uncertainty of our cross-section measurements is in the range 30–35%. As outlined in Section 2.1 an additional uncertainty (5–10%) has to be taken into account in cases where the signal vs exit slit width plot displayed only a poor plateau. For the 446Å emission feature an error of 65% is stated, since the quantum yield at this wavelength is only poorly determined by a linear interpolation between the He II and He I calibration points (see Fig. 2).*

One uncertainty in the measured line emission cross-sections is the extent of the influence of cascade from more highly excited levels. No data was available to allow corrections to be made to the measurements to allow for this effect, but reference to Bashkin and Stoner (1975) suggested that it was likely to be small or negligible in most cases. In addition, only a very limited amount of transition probability and hence branching ratio data are available (e.g. Pradhan and Saraph, 1977). For these reasons level (as distinct from line) cross-sections have not been presented.

3. RESULTS AND DISCUSSION

In this section emission cross-sections and appearance potentials for nineteen lines in the 450–1050Å

* There are cross section data available for lines below 500Å (e.g. Ar II lines and the strong Ne II doublet at 461Å). However, the accuracy of these data is very questionable.

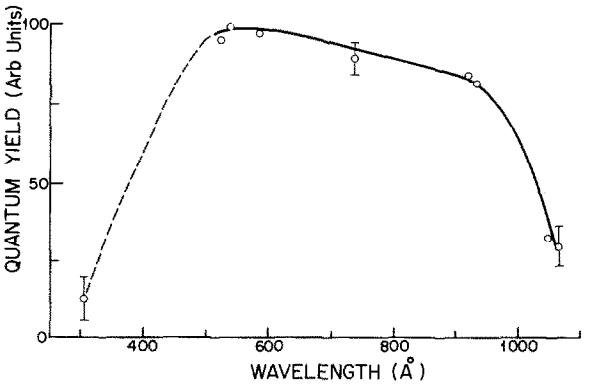

FIG. 2. RELATIVE QUANTUM EFFICIENCY OF THE DETECTION SYSTEM OVER THE WAVELENGTH RANGE INDICATED. Interpolation between the measured points is indicated by the solid line. The dashed line below 500Å indicates the tentative nature of the interpolation in this region. Error bars indicate statistical uncertainties only.

TABLE 2a. CHARACTERISTICS OF O I LINES ARISING FROM THE $nd\ ^3D^\circ$, $(n+1)s\ ^3S^\circ$ EXCITED STATES ($n = 3, 4, 5, 6$)

Observed line in Å	Excited state(s)	Measured onset in eV	Maximum emission cross-section
938*	$6d\ ^3D^\circ + 7s\ ^3S^\circ$	33.0 ± 2.0	$\sim 2.2 \times 10^{-19}$ cm^2 at 150 ± 25 eV
951	$5d\ ^3D^\circ + 6s\ ^3S^\circ$	29.5 ± 1.3	$3.5 \pm 1.3 \times 10^{-19}$ cm^2 at 150 ± 25 eV
972.7†	$4d\ ^3D^\circ$	—‡	$4.0 \pm 1.8 \times 10^{-19}$ cm^2 at 90 ± 10 eV
977.5†	$5s\ ^3S^\circ$	—‡	$3.2 \pm 1.5 \times 10^{-19}$ cm^2 at 180 ± 15 eV
974 (integrated)†	$4d\ ^3D^\circ + 5s\ ^3S^\circ$	30.6 ± 1.5	$6.0 \pm 2.7 \times 10^{-19}$ cm^2 at 150 ± 20 eV
1027	$3d\ ^3D^\circ$	31.4 ± 2.0	$9.9 \pm 3.4 \times 10^{-19}$ cm^2 at 90 ± 10 eV
1040	$4s\ ^3S^\circ$	32.0 ± 1.8	$4.5 \pm 1.7 \times 10^{-19}$ cm^2 at 175 ± 20 eV
1027 + 1040 (integrated) §	$3d\ ^3D^\circ + 4s\ ^3S^\circ$	~ 31.5	$12.2 \pm 4.3 \times 10^{-19}$ cm^2 at 120 ± 20 eV

All lines lead to the $2p^4\ ^3P$ ground state of the oxygen atom.

* The observed 938Å emission consists of a superposition of the weak O I multiplets at 937.8Å and 939.0Å, respectively, and of an intense S II doublet at 937.6Å. The onset of the O I contribution is evident from Fig. 4 and the estimated cross section is the result of a tentative deconvolution (for details, see text).

† The separated $^3D^\circ$ and $^3S^\circ$ contributions have been measured independently from the integrated 974Å emission feature.

‡ Due to intensity limitations, the resolved features of the 974Å emission could not be traced down to threshold.

§ The integrated feature is the superposition of the separately recorded $3d$ and $4s$ features.

TABLE 2b. THRESHOLD ENERGIES FOR FORMATION OF VARIOUS PRODUCTS CALCULATED WITH RESPECT TO LOWEST VIBRATIONAL LEVEL OF PARENT $SO_2(\tilde{X}^1A_1)$ ASSUMING THAT THEY POSSESS ZERO TRANSLATIONAL ENERGY

Reaction products	Calculated minimum energy for production (eV)	Observed onset (eV)
$O^*\begin{pmatrix} 4s\ ^3S^\circ \\ 3d\ ^3D^\circ \end{pmatrix} + SO^+(X^2\Pi)$	27.9	32 ± 2
$+ SO^+(a^4\Pi)$	31.1	
$+ S^*(4s\ ^3S) + O(^3P)$	29.9	
$+ S(^3P) + O^*(3s\ ^3S^\circ)$	32.5	
$+ S^+(^4S) + O(^3P)$	33.4	
$+ S(^3P) + O^+(^4S)$	36.6	
$+ S^+(^4S) + O^+(^4S)$	47.0	

TABLE 3. CHARACTERISTICS OF THE REMAINING O I LINES

Observed line (Å)	Excited State	Measured onset in eV	Maximum emission cross-section
768*	$4d'\ ^3P^\circ$	44.4 ± 1.8	$2.2 \pm 0.7 \times 10^{-19}$ cm^2 at 180 ± 20 eV
811	$3d'\ ^3P^\circ$	41.7 ± 1.8	$2.3 \pm 0.7 \times 10^{-19}$ cm^2 at 150 ± 30 eV
878	$3s''\ ^3P^\circ$	38.5 ± 1.5†	$2.1 \pm 0.8 \times 10^{-19}$ cm^2 at 90 ± 10 eV
989	$3s'\ ^3D^\circ$	33.5 ± 1.6	$9.5 \pm 3.2 \times 10^{-19}$ cm^2 at 110 ± 10 eV

All lines lead to the $2p^4\ ^3P$ ground state of the oxygen atom.

* The emission feature may also contain second order contributions from the O III ($3d'\ ^1F$, $3d'\ ^1D \rightarrow 2p^3\ ^1D^\circ$) transitions at 383Å.

† A weak non-zero intensity was detectable down to approx. 33 eV. However, no distinct additional onset could be attributed to this signal.

TABLE 4. CHARACTERISTICS OF THE O II EMISSION LINES

Observed line in Å	Excited state and transition	Measured onset in eV	Maximum emission cross-section
446	$3d'\ ^2F \rightarrow 2p^3\ ^2D^\circ$	53.1 ± 1.5	$1.5 \pm 1.0 \times 10^{-19}$ cm^2 at 150 ± 20 eV*
539	$3s\ ^4P \rightarrow 2p^3\ 4S^\circ$	39.3 ± 1.5	$0.87 \pm 0.27 \times 10^{-19}$ cm^2 at 320 ± 50 eV
673	$3s\ ^2P \rightarrow 2p^3\ ^2P^\circ$	45.2 ± 1.7	$1.6 \pm 0.5 \times 10^{-19}$ cm^2 at 240 ± 50 eV
719	$2p^4\ ^2D \rightarrow 2p^3\ ^2D^\circ$	42.1 ± 1.4	$1.2 \pm 0.35 \times 10^{-19}$ cm^2 at 220 ± 20 eV
834†	$2p^4\ ^4P \rightarrow 2p^3\ ^4S^\circ$ (O II)	43.3 ± 1.5	
and	$2p^3\ ^3D^\circ \rightarrow 2p^3\ ^3P$ (O III) $4s\ ^3P^\circ \rightarrow 3p^2\ ^1P^\circ$ (S III)	68.0 ± 2.5	$3.7 \pm 1.3 \times 10^{-19}$ cm^2 at 225 ± 40 eV

* The large uncertainty of $\pm 65\%$ is mainly due to the uncertainty in the quantum yield at 446Å, which has been determined by interpolation between the calibration points He I at 522Å and He II at 304Å (see Fig. 2).

† See text for discussion of this feature.

TABLE 5. CHARACTERISTICS OF S II AND S III EMISSION LINES

Observed line in Å	Excited state and transition	Measured onset in eV	Maximum emission cross-section
682Å	$3d\ ^3D^\circ$, $4s\ ^3P^\circ \rightarrow 3p^2\ ^3P$ (S III)	61.0 ± 2.0	$1.8 \pm 0.7 \times 10^{-19}$ cm^2 at 320 ± 30 eV
867	$^2P(?)^* \rightarrow 3p^3\ ^2P^\circ$ (S II)	42.8 ± 1.7	$1.8 \pm 0.5 \times 10^{-19}$ cm^2 at 160 ± 30 eV
910	$4s\ ^4P \rightarrow 3p^3\ ^4S^\circ$ (S II)	38.2 ± 1.3†	$10.4 \pm 3.1 \times 10^{-19}$ cm^2 at 130 ± 15 eV‡
938§	$4s'\ ^2D \rightarrow 3p^3\ ^2D^\circ$ (S II)	42.0 ± 2.5	6.6×10^{-19} cm^2 at 140 ± 20 eV
998	$3d\ ^2F \rightarrow 3p^3\ ^2D^\circ$ (S II)	45.0 ± 1.4	$3.1 \pm 1.2 \times 10^{-19}$ cm^2 at 160 ± 30 eV

* The excited state has not been unambiguously identified. It is believed (Bashkin and Stoner, 1975) that the transition arises from an upper ^2P state.

† A weak non-zero signal extends down to 34 eV. This tail is probably due to a finite distribution of excess kinetic energy of the departing fragments.

‡ There is structure in the energy dependence of the cross-section around 100 eV. This might be a contribution due to the S III ($3p^3\ ^1P^\circ \rightarrow 3p^3\ ^1S$) transition at 911.8Å (see text).

§ See footnote (*) of Table 2a and text.

range are presented, possible underlying processes leading to the emission of a particular line are discussed, and the relevance of the data in view of *Voyager's* recordings is outlined.

3.1. O I *Emissions*

The most prominent O I emission feature is a sequence of multiplets due to the $nd\ ^3D^\circ$, $(n+1)s\ ^3S^\circ \rightarrow 2p^4\ ^3P$ transitions ($n = 3, 4, 5, 6$). The d and s features are well resolved for $n = 3$ (1027 and 1040Å) and just resolved for $n = 4$, where the mutual separation has declined to 4.8Å. As shown in Fig. 3a the energy dependence of the s and d cross-sections is quite different. The transitions from the nd levels display a rather pronounced maximum around 90 eV, which is about 3 times the threshold energy, whereas a comparatively broad maximum at a distinctly higher energy is characteristic of the excitation of the ns levels. A possible reason could be that underlying optically forbidden and electron exchange processes in the parent SO_2 molecule play a more prominent role in the emission of the d-features.

The ratio of the measured emission cross-sections from the $3d$ and $4d$ levels suggests that these emission cross-sections follow quite closely an n^{-3} law. For excitation of the $ns\ ^3S^\circ \rightarrow 2p^4\ ^3P$ lines the fall off in the emission cross-sections is not as rapid being approx. n^{-2}.

In the case of the $ns\ ^3S^\circ$ levels, sufficient transition probability data was available (Pradhan and Saraph, 1977) to enable the level cross sections to be obtained from our measurements. These were approx. fifteen percent larger than our measured line cross-sections. Insufficient branching-ratio information was available in the case of the $nd\ ^3D^\circ$ levels to allow these level cross-sections to be estimated. Cascade is apparently not a problem for any of these levels (Bashkin and Stoner, 1975; Striganov and Sventitskii, 1968).

Figure 3b shows the emission cross-sections of the integrated $[nd+(n+1)s]$ line features. For $n = 3$ the cross-sections of the resolved emissions have simply been added, whereas for $n = 4$ an independent measurement of the integrated blend is presented. The lower (dashed) curve for $n = 6$ is the result of a tentative deconvolution of the complex 938Å emission which consists not only of the O I $[6d\ ^3D^\circ + 7s\ ^3S^\circ] \rightarrow 2p^4\ ^3P$ multiplets, but also of a strong S II $4s'\ ^2D \rightarrow 3p^3\ ^2D^\circ$ contribution. Figure 4 displays the near threshold region of the 938Å excitation function and the two onsets are evident. The first one is due to the oxygen contribution while the second one can be attributed to S II. The deconvolution was based on the assumption that the energy dependence of the O I contribution is similar to that of the 951Å emission ($n = 5$), and the magnitude of the cross-section was taken as the sum of the individual $6d$ and $7s$ line emission cross-sections determined assuming n^{-3} and n^{-2} dependencies for the lines from the d and s states respectively. Justification for this approach comes from the fact that the calculated maximum cross-section for the $n = 5$ emission, making the same assumptions, is 3.4×10^{-19} cm^2 compared to the measured value of 3.5×10^{-19}

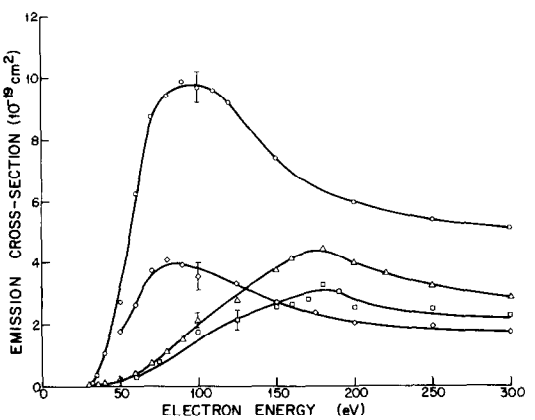

FIG. 3a. VARIATION OF EMISSION CROSS-SECTION WITH INCIDENT ELECTRON ENERGY FOR VARIOUS O I LINES.
Top curve, circles, 1027Å ($3d\ ^3D^\circ$); diamonds, 973Å ($4d\ ^3D^\circ$); triangles, 1040Å ($4s\ ^3S^\circ$), bottom curve, squares, 978Å ($5s\ ^3S^\circ$). Error bars indicate statistical uncertainties.

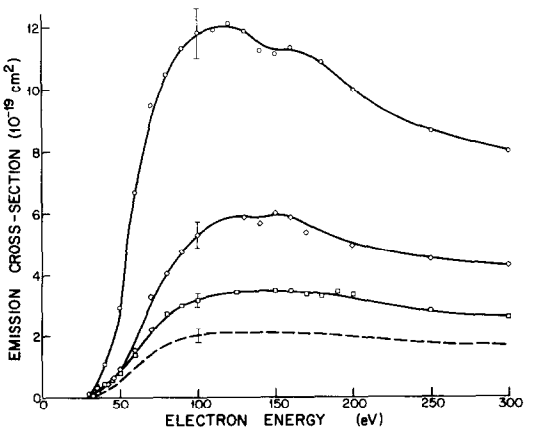

FIG. 3b. VARIATION OF EMISSION CROSS-SECTION WITH INCIDENT ELECTRON ENERGY OF THE COMBINED $[nd\ ^3D^\circ + (n+1)s\ ^3S^\circ] \rightarrow 2p^4\ ^3P$ FEATURES OF O I.
Circles, $n = 3$; diamonds, $n = 4$; squares, $n = 5$; dashed curve, $n = 6$. This last curve was obtained by a deconvolution procedure discussed in the text. Error bars indicate statistical uncertainties.

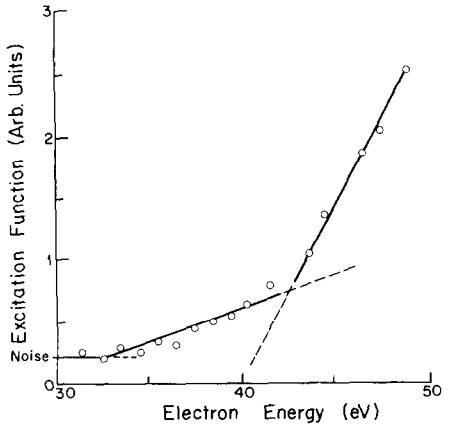

FIG. 4. THRESHOLD REGION EXCITATION OF THE FEATURE AT 938Å.
Two onsets are clearly visible, the one at lower energy is due to O I excitation while the higher onset is due to S II excitation as discussed in text.

cm^2. The two upper curves in Fig. 3b exhibit a double peak reflecting the different energy dependence of the contributing features. Due to the predominant $3d$ feature in the upper curve the lower energy maximum is more pronounced, whereas for $n = 4$ the $4d$ and $5s$ emissions are roughly of equal intensity which results in a very broad maximum with only a slight indication of structure. For higher principle quantum numbers the double peak is completely smeared out. The data for the O I lines arising from the $nd\ ^3D^\circ$ and $(n+1)s\ ^3S^\circ$ excited levels are summarized in Table 2a.

The basic similarity in the shapes within the ns and the nd families of curves suggests that excitation of a given family is proceeding by basically similar processes. We will, therefore, confine our discussion to the lowest members of the family, $4s$ and $3d$ respectively. Table 2b shows some calculated threshold energies (data taken from Herzberg, 1950 and Dujardin and Leach, 1981), for various possible processes assuming no vibrational excitation of the fragments (if molecular) or translational kinetic energy. The observed onsets occur close to 32 eV. Experience with fragmentation processes in other triatomic molecules such as CO_2 or N_2O (Allcock and McConkey, 1976, 1978) demonstrated that translational kinetic energies of a few eV are quite likely and thus it is possible to exclude the processes (Table 2b) in which total fragmentation occurs with simultaneous ionization of either an S or O atom, at least at threshold. This leaves two general classes of processes which are energetically attractive—in the one case the excited O atom is accompanied by an SO^+ ion while in the other total fragmentation occurs with simultaneous excitation of one of the other fragments. The work of Dujardin and Leach (1981) on photoionization of SO_2 reveals that SO^+ is the dominant ion produced. The evidence of Fig. 3a shows that $O(4s\ ^3S^\circ)$ is produced by an optically allowed channel so tentatively we suggest that the ns states are populated by initial excitation of a singlet parent repulsive state followed by decay into $SO^+ + O^*$. The different character of nd-state excitation might be explained if in this case total fragmentation was dominating the production processes with simultaneous excitation of one of the other fragments. A photon–photon coincidence experiment would be needed to unambiguously confirm this. Very recently Orient and Srivastava (1982) have reported electron impact ionization cross-sections of SO_2 indicating that the cross-section for production of the SO^+ fragment ion is much larger than the cross-section for the production of any other fragment ion.

We identified four additional emissions due to O I in our spectrum. The characteristic data for these lines are listed in Table 3 and the emission cross-sections as a function of incident electron energy are displayed in Fig. 5. These excited states belong to a different family to those discussed previously being based on *excited* parent O^+ cores. The energy dependence of the 878 and 989Å emission cross-sections displays a steep increase above a threshold close to 33 eV to a marked maximum at rather low impact energies, which could reflect a contribution from underlying optically forbidden processes. This is very similar to what was observed with the excitation of the $nd\ ^3D^\circ$ states discussed earlier, so perhaps similar processes mainly involving total fragmentation are responsible. This is certainly

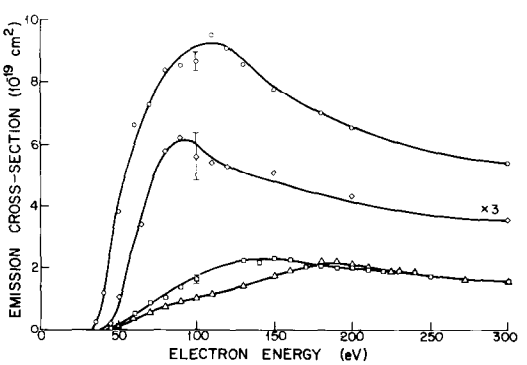

FIG. 5. VARIATION OF EMISSION CROSS-SECTION WITH INCIDENT ELECTRON ENERGY FOR VARIOUS O I EMISSIONS.
Top curve, circles, 989Å ($3s'\ ^3D^\circ \rightarrow 2p^4\ ^3P$); diamonds, 878Å ($3s''\ ^3P^\circ \rightarrow 2p^4\ ^3P$), please note that this curve has been multiplied by a factor 3 for clarity of presentation; squares, 811Å ($3d'\ ^3P^\circ \rightarrow 2p^4\ ^3P$); bottom curve, triangles, 768Å ($4d'\ ^3P^\circ \rightarrow 2p^4\ ^3P$). Error bars indicate statistical uncertainties.

consistent with the energy data (Table 2b) remembering that an additional 0.5 (2.1) eV is required to excite the 989Å (878Å) line over that required for 1027/1040Å. The 768Å and 811Å cross sections were found to rise gradually from threshold to a broad maximum and a rather slow fall-off towards higher impact energies pointing to purely optically allowed excitation processes in the parent SO_2 molecule. The measured onset potentials above 40 eV strongly suggest that total fragmentation was also occurring in this case though this time via singlet parents only. Note that the 768 and 811Å features arise from the same family of excited states, $4d'\ ^3P^\circ$ and $3d'\ ^3P^\circ$ respectively. The difference in the shapes of the cross-sections above 100 eV is probably due to an additional second order contribution to the 768Å feature from two O III lines at 383Å. These would have a minimum appearance potential of around 106 eV.

There were no significant O I contributions in the spectra recorded during *Voyager's* mission. The plasma torus around Jupiter does not emit any radiation in the 900–1000Å range and an emission feature around 1020Å was attributed to the S III ($3p^3\ ^3P^\circ \rightarrow 3p^2\ ^3P$) rather than to the nearby O I ($3d\ ^3D^\circ \rightarrow 2p^4\ ^3P$) transition. On the other hand, we found only a very weak emission at 1020Å in our wavelength scan roughly 1/30 and 1/10 of the intensity of the 1027Å features at incident impact energies of 100 and 400 eV, respectively. Clearly, therefore, single step excitation of these features is not occurring in the torus.

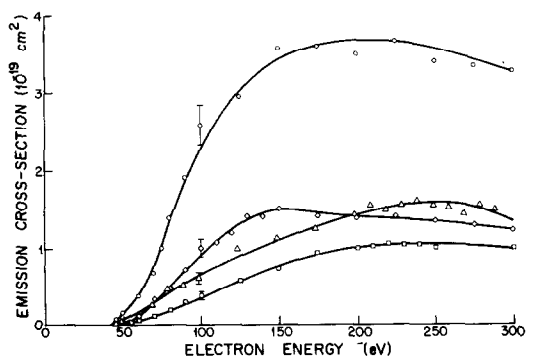

FIG. 6. VARIATION OF EMISSION CROSS-SECTION WITH INCIDENT ELECTRON ENERGY FOR VARIOUS O II EMISSIONS.
Top curve, circles, 834Å ($2p^4\ ^4P \rightarrow 2p^3\ ^4S^\circ$); diamonds, 446Å ($3d'\ ^2F \rightarrow 2p^3\ ^2D^\circ$); triangles, 673Å, ($3s\ ^2P \rightarrow 2p^3\ ^2P^\circ$); bottom curve, squares, 719Å, ($2p^4\ ^2D \rightarrow 2p^3\ ^2D^\circ$). Note that the 834Å curve also contains contributions from O III ($2p^3\ ^3D^\circ \rightarrow 2p^3\ ^3P$) and possibly S III ($4s\ ^3P^\circ \rightarrow 3p^2\ ^1P^\circ$). See discussion in text and onset data, Fig. 7. Error bars indicate statistical uncertainties.

3.2. *Emissions from ionized oxygen*

We measured emission cross sections for the five O II features listed in Table 4. All lines except the 834Å blend, which is a complex superposition of two or three multiplets, appeared to be rather weak. In Fig. 6 all the measured emission cross-sections are shown except for the 539Å line, which displays the maximum cross section above 300 eV and is presented together with the S III 682Å feature in Fig. 9. The energy dependence of all O II cross-sections points to optically allowed excitation in the SO_2 molecule since no pronounced maxima at low impact energies have been found. The onset potentials of 40–45 eV identify the dissociation paths leading to the 446, 539, 673 and 719Å emissions uniquely as the partial fragmentation $SO_2 \rightarrow SO + O^{+}*$. Total fragmentation with excitation of these states would require energies of 45–55 eV.

A detailed look into the low energy region of the 834Å excitation function (Fig. 7) reveals that at least two components contribute to the emission of this feature. There is a first onset around 43 eV which is probably due to the O II ($2p^4\ ^4P \rightarrow 2p^3\ ^4S^\circ$) transition at 833.5Å. Energetically this excitation could be accompanied by either partial or total fragmentation. Superimposed on the increasing flank of the O II excitation function there is evidence of a second onset with an appearance potential of 68 eV. This additional contribution can be attributed to the

$$\text{O III } (2p^3\ ^3D^\circ \rightarrow 2p^3\ ^3P,\ 834.3\text{Å})$$

and the

$$\text{S III } (4s\ ^3P^\circ \rightarrow 3p^2\ ^1P^\circ,\ 836.3\text{Å})$$

transitions. The S III line is an intercombination line and, therefore, is probably rather weak. If we assume that its contribution is negligible and that the underlying O II line has an emission cross section similar in shape to the other O II lines, Fig. 6, then an approximate deconvolution of the O III contribution can be made. When this is done, the maximum in the O III emission cross-section is approx. 1.5×10^{-19} cm^2 around 150 eV. It is interesting to note that both the 719 and 834Å O II features and the 834Å O III line are the result of not only fragmentation of the SO_2 but also ejection of an inner shell (2*s*) electron from the O-atom or ion.

O II transitions were found to appear only weakly in the spectra recorded by *Voyager's* spectrometers, suggesting that excitation of this species by indirect mechanisms is even weaker than by the direct mechanisms which we were probing. The strong feature at 833Å recorded by *Voyager* was concluded to be predominantly O III.

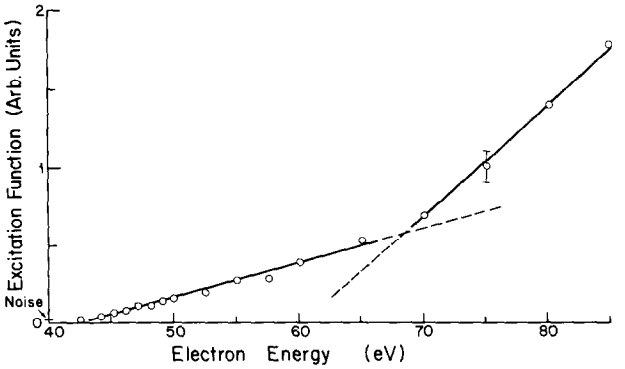

FIG. 7. THRESHOLD REGION EXCITATION OF THE 834Å FEATURE.
Note the two onsets around 43 eV (O II excitation) and 68 eV (O III and S III excitation).

3.3. *S II and S III emissions*

Since radiation arising from sulphur fragments probably requires initially a total fragmentation of the parent SO_2 molecule and since emissions in the spectral range of our interest are due to ionic sulphur species only, the appearance potentials given in Table 5 are comparatively high. The differences between the measured appearance potentials and the calculated minimum energies are quite small suggesting that the kinetic energies of the fragments are likewise small. A weak non-zero signal was found to extend from about 34 eV to the sharp onset of the 910Å excitation function around 38 eV. The minimum energy to produce total fragmentation with excitation of S II (910Å) is 35 eV. This tail, therefore, might be due to a finite distribution of excess kinetic energy of the departing fragments.

Figure 8 shows the emission cross sections as a function of electron energy for the S II multiplets. The 910Å curve displays a structure around 100 eV which indicates either the existence of another strong production process or possibly it might be attributed to the S III ($3p^3\ ^1P^\circ \rightarrow 3p^3\ ^1S$) transition at 911.8Å with an onset potential in the 80–90 eV range. Included in Fig. 8 are the measured points of the complex (S II + O I) 938Å emission as well as the deconvoluted S II contribution (dashed curve). Details of the deconvolution are outlined in Section 3.1. The energy dependence of the S II emission cross-sections is typical of predominantly optically allowed excitation processes in the parent SO_2 molecule.

The S III 682Å emission cross-section is presented in Fig. 9 together with the O II 539Å line. Both emission cross sections are small in magnitude and display a very smooth energy dependence with a broad maximum slightly above 300 eV. There is some indication of structure with an onset around 200 eV in the 682Å curve. An additional onset at such a high energy would require the simultaneous formation of highly ionized fragments in the underlying process.

The most intense S II emissions were found in the 900–1000Å spectral range, where as previously mentioned almost no radiation was observed by *Voyager's* spectrometers. On the other hand, the prominent S III multiplets in the spectra emitted by the plasma torus at 700, 825 and 1020Å and the S IV ($3p^2\ ^2D \rightarrow 3p\ ^2P^\circ$) transition at 1070Å were hardly detectable in our spectra; only slight indications were found in the 400 eV wavelength scan, but were so weak that no individual cross sections could be measured. The bright feature around 685Å from the plasma torus is believed to consist of a blend of S III multiplets at 680,

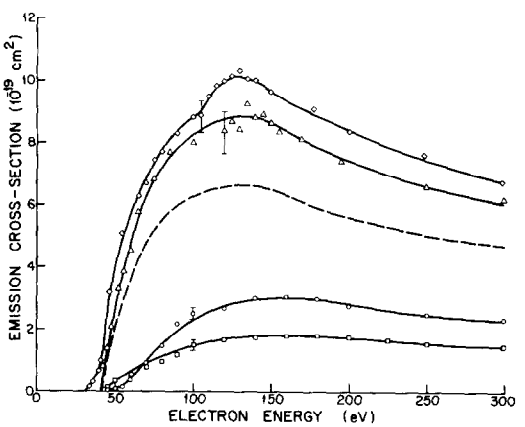

FIG. 8. VARIATION OF EMISSION CROSS-SECTION WITH INCIDENT ELECTRON ENERGY FOR VARIOUS S II AND S III EMISSIONS.
Top curve, diamonds, 910Å ($4s\ ^4P \rightarrow 3p^3\ ^4S^\circ$); triangles, 938Å—this feature contains a contribution from O I lines, the dashed curve gives S II ($4s'\ ^2D \rightarrow 3p^3\ ^2D^\circ$) after the O I contribution has been subtracted, see text; circles, 998Å ($3d\ ^2F \rightarrow 3p^3\ ^2D^\circ$); bottom curve, squares, 867Å, ($^2P \rightarrow 3p^2\ ^2P^\circ$). Error bars indicate statistical uncertainties.

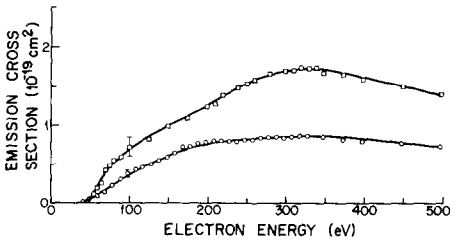

FIG. 9. VARIATION OF EMISSION CROSS-SECTION WITH INCIDENT ELECTRON ENERGY FOR 682Å, S III, ($3d\ ^3D^\circ$, $4s\ ^3P^\circ \rightarrow 3p^2\ ^3P$), UPPER CURVE AND SQUARES, AND 539Å O II ($3s\ ^4P \rightarrow 2p^3\ ^4S^\circ$), LOWER CURVE AND CIRCLES, EMISSIONS.
Error bars indicate statistical uncertainties.

683 and 700Å with a small contribution due to the O III ($2p^3\ ^3P^\circ \rightarrow 2p^2\ ^3P$) transition at 703Å. Under our laboratory conditions only negligible emissions around 700Å were found and the superposition of the S III multiplets at 680 and 683Å apparently gives rise to the feature centred at 682Å. The 685Å blend was by far the most intense emission in the spectra recorded during *Voyager's* mission, whereas the 682Å feature was among the weaker emissions produced in our experiment with a maximum cross section of only 1.8 $\times 10^{-19}$ cm^2. All of this again highlights the fact that the excitation of the emissions from the torus must proceed indirectly in a number of steps.

Acknowledgements—The authors gratefully acknowledge financial assistance from the Natural Sciences and Engineering Research Council of Canada. One of us (K.B.) wishes to acknowledge financial aid from the Deutsche Forschungsgemeinschaft (DFG). John C. Huschilt took some of the preliminary data.

REFERENCES

Allcock, G. and McConkey, J. W. (1976) Metastable fragment production following electron impact on CO_2. *J. Phys. B: Atom. Molec. Phys.* **9**, 2127.

Allcock, G. and McConkey, J. W. (1978) Dissociation patterns in N_2O following electron impact. *Chem. Phys.* **34**, 169.

Bashkin, S. and Stoner, J. O. (1975) *Atomic Energy Levels and Grotrian Diagrams.* North Holland, Amsterdam.

Bloemen, E. W. P., Winter, H., Märk, T., Dijkkamp, D., Barrends, D. and de Heer, F. J. (1981) Absolute emission cross sections at 30.4 nm for e-He collisions and at 20.8 nm for Ne^{4+}-He collisions. *J. Phys. B: Atom. Molec. Phys.* **14**, 717.

Broadfoot, A. L., Belton, M. J. S., Takacs, P. Z., Sandel, B. R., Shemansky, D. E., Holberg, J. B., Ajello, J. M., Atreya, S. K., Donahue, T. M., Moos, H. W., Bertaux, J. L., Blamont, J. E., Strobel, D. F., McConnel, J. C., Dalgarno, A., Goody, R. and McElroy, M. B. (1979) Extreme ultraviolet observations from *Voyager* 1 encounter with Jupiter. *Science* **204**, 979.

Donaldson, F. G., Hender, M. A. and McConkey, J. W. (1972) VUV measurements of the electron impact of He. *J. Phys. B: Atom. Molec. Phys.* **5**, 1192.

Dujardin, G. and Leach, S. (1981) Photonion-fluorescence photon coincidence study of radiative and dissociative relaxation processes in VUV photoexcited SO_2; fluorescence of SO_2^+, SO^+ and SO. *J. chem. Phys.* 75, 2521.

Flicker, W. M., Mosher, O. A. and Kuppermann, A. (1978) Electron-impact excitation of low-lying electronic states in CS_2, OCS and SO_2. *J. chem. Phys.* **69**, 3910.

Foo, V. Y., Brion, C. E. and Hasted, J. B. (1971) Electron energy-loss spectra of some triatomic molecules, *Proc. R. Soc., London* **A22**, 535.

Herzberg, G. (1950) *Molecular Spectra and Molecular Structure.* Vol. I–III. Van Nostrand Reinhold, New York.

McConkey, J. W. and Donaldson, F. G. (1973) Excitation of the resonance lines of Ar by electrons. *Can. J. Phys.* **51**, 914.

Orient, O. J. and Srivastava, S. K. (1982) Mass spectrometric determination of partial and total electron impact ionization cross-sections from threshold up to 200 eV. *VIII ICAP, Abstracts of Contributed Papers.* Wallin & Dalholm, Lund.

Pradhan, A. K. and Saraph, H. E. (1977) Oscillator strengths for dipole transitions in neutral oxygen. *J. Phys. B: Atom. Molec. Phys.* **10**, 3365.

Reese, R. M., Dibeler, V. H. and Franklin, J. L. (1958) Electron impact studies of sulphur dioxide and sulphuryl fluoride. *J. chem. Phys.* **29**, 880.

Sandel, B. R., Shemansky, D. E., Broadfoot, A. L., Bertaux, J. L., Blamont, J. E., Belton, M. J. S., Ajello, J. M., Holberg, J. B., Atreye, S. K., Donahue, T. M., Moos, H. W., Strobel, D. F., McConnel, J. C., Dalgarno, A., Goody, R., McElroy, M. B. and Takacs, P. Z. (1979) Extreme ultraviolet observations from *Voyager* 2 encounter with Jupiter. *Science* **206**, 962.

Smith, O. I. and Stevenson, J. S. (1981) Determination of cross-sections for formation of parent and fragment ions by electron impact from SO_2 and SO_3. *J. chem. Phys.* **74**, 6777.

Smyth, H. D. and Mueller, D. W. (1932) The ionization of sulphur dioxide by electron impact. *Phys. Rev.* **43**, 121.

Srivastava, S. K. and Ajello, J. M. (1981) Dissociative excitation of SO_2 by electron impact. XII ICPEAC, abstracts of contributed papers. North Holland, Amsterdam.

Stringanov, A. R. and Sventitskii, N. S. (1968) *Tables of Spectral Lines of Neutral and Ionized Atoms.* Plenum Press, New York.

Tan, K-H., Donaldson, F. G. and McConkey, J. W. (1974) Excitation of the $3s\,3p^6\ ^2S$ and $3s^2\,3p^4\,4s\ ^2P$ levels of Ar^+ and the 736Å line of Ne by electrons. *Can. J. Phys.* **52**, 786.

van Eck, J. and de Jongh, J. P. (1970) Determination of absolute cross-sections for excitation of n^1P levels of He by electron impact (30–1000 eV). *Physica* **47**, 141.

Vuskovic, L. and Trajmar, S. (1981) The electron impact spectra of SO_2. *J. Raman Spectry.* **10**, 136.

Westerveld, W. B., Heideman, H. G. M. and van Eck, J. (1979) Electron impact excitation of $1^1S \rightarrow 2^1P$ and $1^1S \rightarrow 3^1P$ of helium: excitation cross sections and polarization fractions obtained from XUV radiation. *J. Phys. B: Atom. Molec. Phys.* **12**, 115.